NEOPLASIA
www.neoplasia.com

Volume 13 Number 8 August 2011 pp. 692–703 692

Persistent Inflammation Leads to Proliferative Neoplasia and Loss of Smooth Muscle Cells in a Prostate Tumor Model[1,2]

Andreas Birbach*, David Eisenbarth*, Nicolas Kozakowski†, Eva Ladenhauf*, Marc Schmidt-Supprian‡ and Johannes A. Schmid*

*Department of Vascular Biology and Thrombosis Research, Medical University of Vienna, Vienna, Austria; †Clinical Institute of Pathology, Medical University of Vienna, Vienna, Austria; ‡Max Planck Institute of Biochemistry, Martinsried, Germany

Abstract

In prostate cancers, epidemiological data suggest a link between prostate inflammation and subsequent cancer development, but proof for this concept in a tumor model is lacking. A constitutively active version of IκB kinase 2 (IKK2), which is activated by many inflammatory stimuli, was expressed specifically in the prostate epithelium. Constitutive activation of the IKK2/nuclear factor κB axis was insufficient for prostate transformation. However, in combination with heterozygous loss of phosphatase and tensin homolog, IKK2 activation led to an increase in tumor size, formation of cribriform structures, and increase in fiber in the fibroblastic stroma. This phenotype was coupled with persistent inflammation evoked by chemokine expression in the epithelium and stroma. The hyperplastic and dysplastic epithelia correlated with changes evoked by decreased androgen receptor activation. Conversely, inflammation correlated with stromal changes highlighted by loss of smooth muscle cells around prostate ducts. Despite the loss of the smooth muscle barrier, tumors were rarely invasive in a C57BL/6 background. Data mining revealed that smooth muscle markers are also downregulated in human prostate cancers, and loss of these markers in primary tumors is associated with subsequent metastasis. In conclusion, our data show that loss of smooth muscle and invasiveness of the tumor are not coupled in our model, with inflammation leading to increased tumor size and a dedifferentiated stroma.

Neoplasia (2011) 13, 692–703

Introduction

Inflammation as a causal agent has been linked to approximately 20% of human cancers [1]. The type and nature of inflammatory infiltrates are different for different cancer types, and thus, a number of different mechanisms for the tumor-promoting effect of inflammation have been proposed [2]. In prostate cancer, a growing amount of evidence suggests a link between chronic or persistent inflammation and tumor development [3]. First, epidemiological data indicate that people diagnosed with chronic prostatitis have an increased risk of developing prostate cancer at a later age. Moreover, people receiving long-term treatment with nonsteroidal anti-inflammatory drugs have a reduced risk of developing prostate cancer [4–6]. Second, histologic data imply that certain lesions (sometimes referred to as prostate inflammatory atrophy) are frequently found near prostate intraepithelial neoplasias (PINs), precursor lesions of prostate cancer [7]. Third, treatment of rodent prostates with bacteria induces prostatitis and hyperplastic and dysplastic epithelial alterations [8,9]. Although all these data suggest a link between prostatitis and tumor formation, the cause of prostate inflammation in humans is largely unknown. However, many possible causes for an inflammatory phenotype, such as bacterial or viral infections or production of inflammatory cytokines and chemokines, share

Abbreviations: AR, androgen receptor; IKK2, IκB kinase 2; PTEN, phosphatase and tensin homolog; SMA, smooth muscle actin

Address all correspondence to: Andreas Birbach, PhD, Department of Vascular Biology and Thrombosis Research, Medical University of Vienna, Schwarzspanierstrasse 17, A-1090 Vienna, Austria. E-mail: andreas.birbach@meduniwien.ac.at

[1]This work was supported by a grant from the Austrian Science Fund FWF (P21919-B13 to A.B.).

[2]This article refers to supplementary materials, which are designated by Tables W1 to W4 and Figures W1 to W5 and are available online at www.neoplasia.com.

Received 13 April 2011; Revised 9 June 2011; Accepted 13 June 2011

DOI 10.1593/neo.11524

common signaling pathways that are activated in the affected tissue. All of the aforementioned stimuli activate the IκB kinase 2 (IKK2), a key mediator between extracellular signaling and the transcription factor NF-κB [10]. Although IKK2 has some other targets, its main function is phosphorylation of IκB (inhibitors of κB) molecules, rendering them subject for degradation and thus activating NF-κB. Moreover, IKK2 has been described as an oncogenic kinase; activated IKK2 correlates with poor clinical outcome in breast cancer patients, and the enzyme targeting IKK2 for ubiquitination and degradation is lost or mutated in different human cancers [11,12]. For the prostate, it is interesting to note that the aforementioned relationship between long-term drug treatment and reduced prostate cancer risk is more significant for aspirin, which is also an IKK2 inhibitor.

In this work, we describe a novel genetic mouse model for inflammatory signaling in the prostate epithelium based on the expression of a constitutively active version of the IκB kinase 2 (IKK2ca). Using the Cre/LoxP system and the well-described Probasin-Cre mice [13], we expressed IKK2ca in epithelial cells of the mouse prostate with or without a monoallelic deletion of the tumor suppressor phosphatase and tensin homolog (PTEN; monoallelic loxP-flanked PTEN) in the same cells. PTEN is a tumor suppressor frequently mutated or lost in prostate cancer. In mouse models, PTEN deficiency in the epithelium shows a dose-dependent transformation of prostate tissue, with low-grade PIN late in mouse life in monoallelic deletions and lesions with ability to form invasive and eventually metastasizing carcinomas in full deletions [14–16]. We wanted to answer the questions whether signaling through IKK2/NF-κB is sufficient to transform prostate tissue and whether IKK2 activation in mild neoplastic lesions can advance tumor formation. We will refer to prostates carrying normal or modified epithelia as wild-type, prostate epithelium (PE–)IKK2ca, PE–PTEN+/–, or PE–PTEN+/–IKK2ca.

Materials and Methods

Mice

Probasin-Cre (PB-Cre4) mice were obtained from the National Cancer Institute – Frederick Mouse Repository. Mice with a floxed PTEN allele [17] were a gift from Prof Tak Mak. R26StopFlIKK2ca mice were generated by one of the authors (M.S.-S.) and were described previously [18]. Mice were bred on a C57BL/6 background. Their housing and euthanasia were in accordance with institutional guidelines.

RNA Extraction and Quantitative Polymerase Chain Reaction Analysis

Harvested tissue was stored in RNA later, then homogenized using a Polytron homogenizer, and purified on RNA binding columns according to the manufacturer's instructions (RNeasy [Qiagen, Hilden, Germany] or Total RNA Kit [Peqlab, Erlangen, Germany]). Complementary DNA (cDNA) synthesis was performed using the RevertAid H Minus First Strand cDNA Synthesis Kit (Fermentas, St. Leon-Rot, Germany) and random hexamer primers. Quantitative polymerase chain reaction (PCR) was done on a StepOne Plus Real-time PCR Cycler (Applied Biosystems, Vienna, Austria). *HPRT* was used as normalization gene. Primer sequences are listed in Table W1.

Microarray Experiment

Total RNA was extracted from lateral prostates of three animals (12 months) with PTEN+/–IKK2ca/ca prostates and three age-matched animals with PTEN+/– prostates using RNeasy (Qiagen). RNA quality control, labeling, hybridization, and initial data analysis were done by an Affymetrix service provider (KFB Regensburg, Regensburg, Germany). Complete array data are stored in GEO (accession no. GSE26410). For presentation in tables, $\log_2$ signals from the Robust Multichip Analysis were transformed into linear signals, and the mean expression fold was calculated by dividing the average signal from the PE–PTEN+/–IKK2ca/ca by the average signal from the PE–PTEN+/– group.

Explant Culture

Dissected prostate tissue was cut into pieces of 0.2 to 1 mm, placed on collagenated tissue culture plates, and supplied with minimal amount of epithelial growth medium containing 1% serum as described by Barclay and Cramer [19]. After 24 hours, more media were added. After further 24 to 48 hours, cells began to grow out from the prostate tissue. Clean epithelial or stromal cultures were obtained by removing the unwanted cell type with a cell scraper or pipette tip. Cells were passaged using Accutase (PAA, Pasching, Austria). For generation of cell lines, cells were passaged until they survived crisis. Cell lines were treated in some experiments with tumor necrosis factor (TNF; 20 ng/ml; Immunotools, Friesoythe, Germany) or BMS-345541 (10 μM; Sigma, Schnelldorf, Germany).

Tissue Sectioning and Immunostaining

For paraffin sections, harvested tissue was fixed overnight in 4% paraformaldehyde. Tissues were then dehydrated, embedded in paraffin in small tissue blocks, cut (2-μm sections) using a Leica microtome (Leica Microsystems, Vienna, Austria), and collected on SuperFrost Plus slides (Thermo Scientific, Braunschweig, Germany). Antibody staining procedure has been described [20]. Apoptosis was assessed using the TUNEL method and the *In Situ* Cell Death Detection Kit (Roche, Vienna, Austria).

For frozen sections, harvested tissue was directly frozen in isopentane/liquid nitrogen and stored at −80°C until cutting. Staining was done as described [20]. For biotinylated antibodies, sections were blocked with Avidin/Biotin Blocking Kit (Vector Laboratories, Burlingame, CA). Antibodies used are described in Table W2.

Histologic Assessment

Hematoxylin and eosin (H&E) staining from paraffin sections was judged in a blind fashion by an expert pathologist (N.K.).

Microscopy and Image Analysis

Images were acquired on an Olympus AX470 microscope (Olympus, Vienna, Austria) equipped with F-View II (grayscale) and ColorViewII (color) digital cameras using the manufacturer's software (CellP; Olympus) and appropriate filter sets for fluorescence.

For the quantification of stromal elements, individual ducts (>5) were randomly chosen on H&E staining of lateral prostates, and the number of fibers between the gland and the neighboring gland was counted. The average number of fibers was calculated for each prostate tissue. The numbers given in the figures represent the arithmetic average and SD over the individual values.

For the quantification of smooth muscle thickness *versus* CD11b count, parameters were quantified using ImageJ (National Institutes of Health, Bethesda, MD). The diameter of smooth muscle was quantified using the anti-actin staining and the line selection of ImageJ. CD11b-positive cells were counted within the duct and in the stroma closer to the investigated duct than the neighboring one and were then normalized to the area of the respective duct.

For quantification of Ki67- and TUNEL-positive cells, polymorphonuclear inflammatory cells were excluded from the analysis.

For quantification of androgen receptor (AR) nuclear/cytoplasmic ratio, AR fluorescent staining was analyzed using elliptical regions inside and just outside the nucleus and determining the mean gray value of the regions in ImageJ. Nuclear regions were identified by overlaying Hoechst staining.

Statistical Analysis

One-way analysis of variance was used to determine statistical significance, where applicable. $P < .05$ was considered statistically significant. Error bars in figures represent SEM.

Results

IKK2 Activity Is Insufficient to Transform Prostate Epithelium

Given the central role of IKK2 as a signal mediator from inflammatory agents to transcription factors and its description as an oncogenic kinase, we wanted to determine whether chronic IKK2 activity leads to transformation of the prostate epithelium. On excision of the Stop cassette in R26StopFlIKK2ca mice, transgene expression was confirmed by means of the Flag-tag of the IKK2 transgene (Figure 1*A*). As expected, the expression was restricted to the epithelium. Dissection of the different prostate lobes and expression analysis using quantitative reverse transcription–polymerase chain reaction (RT-PCR) showed that transgene expression was highest in the lateral prostate, followed by the anterior and dorsal prostates, and was lowest in the ventral prostate (Figure 1*B*). Down-regulation of IκBα, which is degraded after phosphorylation by IKKs, indicated IKK2 activity (Figure 1*C*). However, no histologic phenotype of the prostate tissue was noticed after 4 ($n = 3$), 8 ($n = 4$), or 12 ($n = 10$) months of age either in animals expressing IKK2ca from a single allele or in animals expressing the transgene from both alleles (Figure 1*D*). We conclude that constitutively active IKK2 is insufficient to transform prostate tissue.

IKK2 Activity on PTEN+/– Background Increases Tumor Size and Epithelial and Stromal Proliferation

Transgenic prostates with monoallelic deletion of the PTEN tumor suppressor (PTEN+/–) in the epithelium develop low-grade PIN late in mouse life (around 10-12 months). We wanted to know whether IKK2 signaling could enhance this tumor development and alter either tumor size or invasiveness. Expression of constitutively active IKK2 in PTEN+/– prostate epithelium led to a clearly visible increase in prostate size (Figure 2*A*, after 12 months). The difference was significant after 8 months and not seen at 4 months (not shown). PTEN+/– epithelium expressing IKK2ca on both alleles (IKK2ca/ca) had all prostate lobes enlarged at 8 months and older, whereas PE–PTEN+/–IKK2ca (expressing IKK2ca from one allele) only showed enlarged lateral prostates, in line with transgene expression being highest in the lateral lobe (Figure 2*C*, cf., Figure 1*B*). Histologic staining of these prostates showed normal, smooth epithelium in prostates from wild-type littermates, whereas most PE–PTEN+/– prostates had some hyperplasia and focal nuclear abnormalities judged as murine PIN. PTEN+/– IKK2ca (or ca/ca) epithelium was severely hyperplastic, often leading to cribriform structures,

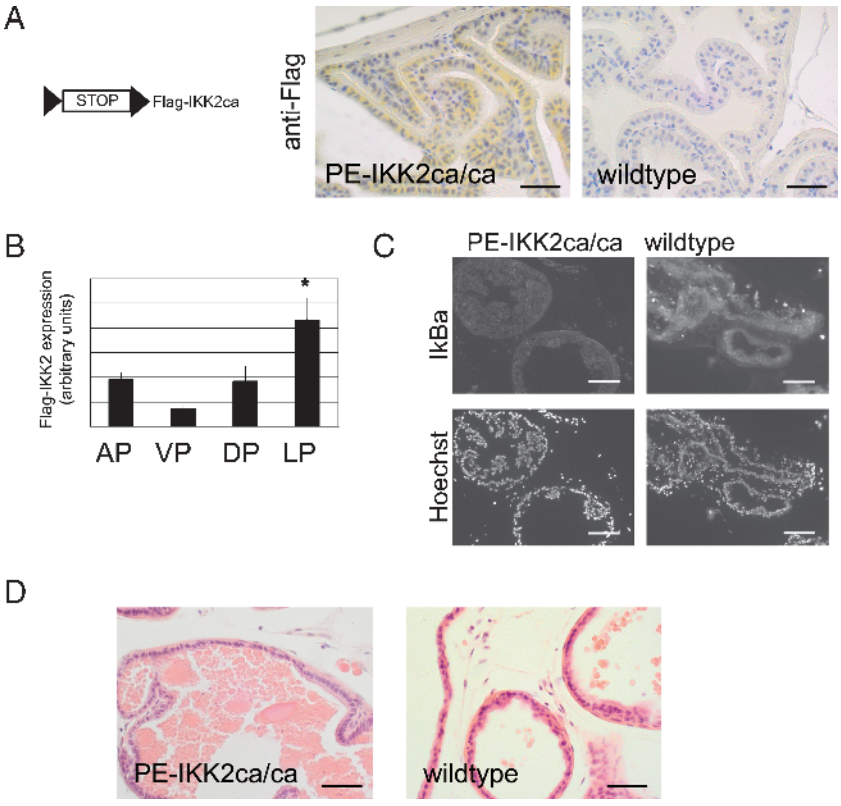

Figure 1. IKK2 signaling is insufficient to transform prostate epithelium. (A) schematic drawing of the R26StopFlIKK2ca mouse line (loxP sites: triangles) and anti-Flag staining. (B) Quantitative RT-PCR for the Flag-IKK2 transgene in different prostate lobes of IKK2ca/ca expressing mice ($n = 4$). (C) Immunostaining of frozen sections of wild-type or PE−IKK2ca/ca prostates with IκBα antibody. (D) H&E stain from lateral prostate of IKK2ca/ca expressing mouse (12 months). Scale bars, 50 μm (A, D); 100 μm (C). Error bars, SEM. *$P < .05$. AP indicates anterior prostate; DP, dorsal prostate; LP, lateral prostate; VP, ventral prostate.

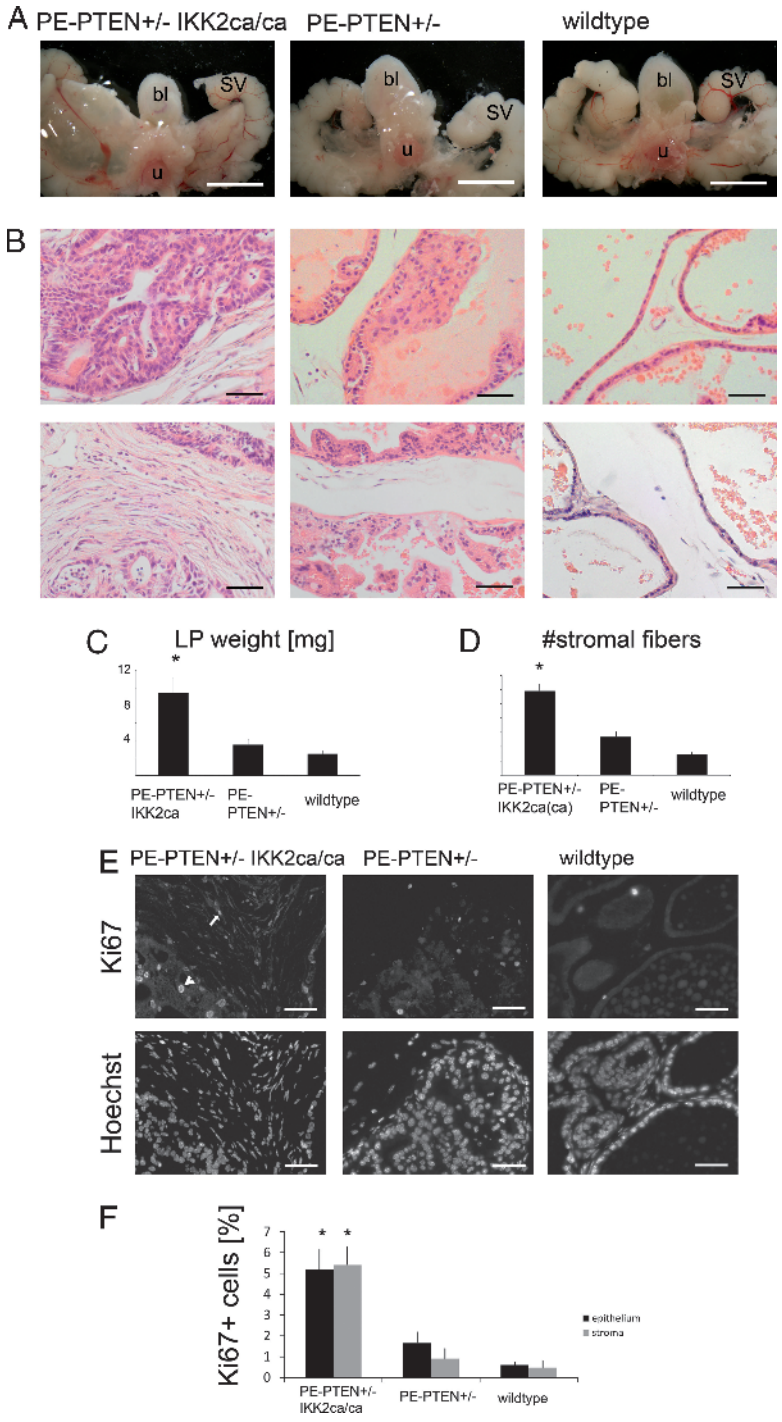

Figure 2. IKK2 activity on PTEN+/− background increases tumor size and epithelial and stromal proliferation. (A) Steromicroscopical images of the structures surrounding the urethra (u), bladder (bl), and seminal vesicles (SV) from 12-month-old mice. The prostate lobes are seen between the noted structures. (B) H&E stain of lateral prostates at 12 months, focusing on epithelium (upper panels) and stroma (lower panels). The genotypes are according to labeling in A. (C) Quantification of dry prostate weight of lateral prostates at 12 months. (D) Stromal fiber number in between epithelial ducts (see Materials and Methods) of 12-month-old lateral prostates. (E) Paraffin sections of lateral prostates (12 months) stained for proliferation marker Ki67. Positive cells in the epithelium (arrowhead) and stroma (arrow) are seen. Hoechst staining of the same sections (lower panels) are given to indicate tissue structure. (F) Quantification of Ki67-positive cells in the epithelium and stroma for the indicated genotypes. Scale bars, 5 mm (A); 50 μm (B, E). Error bars, SEM. *$P < .01$.

but had an equal incidence of nuclear atypia as PTEN+/− epithelium (Figure 2*B*, *upper panels*). Moreover, PE–PTEN+/–IKK2ca(ca) prostates showed a dramatic stromal response, indicated by dense and numerous collagen fibers in comparison to the loose stroma with few fibers in normal or PE–PTEN+/− prostates (Figure 2*B*, *lower panels*, quantified in Figure 2*D*). This increase in tumor size was due to an increase in proliferation of both epithelial and stromal cells, as indicated by more Ki67-positive cells in epithelium and stroma, respectively (Figure 2, *E* and *F*). Apoptosis assessed by TUNEL stain was low and not significantly changed in one of the genotypes (Figure W1).

Persistent Inflammation in PE–PTEN+/– IKK2ca Prostates

The proliferative epithelium and stromal response were coupled with signs of severe prostatitis in PE–PTEN+/– IKK2ca(ca) prostates. Prostate tissue showed infiltration of granulocytes characterized by their polymorphic nuclei and positive staining with the neutrophil marker Lipocalin2 (Figure 3, *A* and *B*). The infiltrates were seen in the stroma but also in the epithelium where they could be easily spotted in the lumina of cribriform structures (Figure 3*A*). Wild-type tissue and younger PE–PTEN+/– (4 months, $n = 3$; 8 months, $n = 5$) were devoid of infiltrates, although with advanced age (>12 months), some PE–PTEN+/– prostates also developed signs of prostatitis (analysis in Figure 3*C*). Immunofluorescence analysis revealed positive staining of infiltrates with the macrophage/monocyte antigen CD11b, the macrophage marker F4/80, and the neutrophil marker Gr-1 (Figure 3*D*). Leukocytes positive for CD3e were also seen but were generally rare (not shown). Control tissues from PE–PTEN+/–IKK2ca/ca mice did not show any signs of inflammation, and noninflamed prostates did not show positive immunoreactivity with immune cell marker antibodies (Figure W2). We conclude that the prostate-specific expression of constitutively active IKK2 on a PE–PTEN+/– background leads to severe persistent inflammation characterized by infiltration of neutrophil granulocytes and macrophages.

Loss of Smooth Muscle but No Invasion in PE–PTEN+/–IKK2ca(ca) Prostates

Because histologic staining of prostate tissue showed a dramatic change in the stroma, we investigated the expression of various candidate genes known or thought to be expressed in the prostate stroma. We found a dramatic down-regulation of smooth muscle cell markers, smooth muscle myosin heavy chain (*MYH11*), and smooth muscle

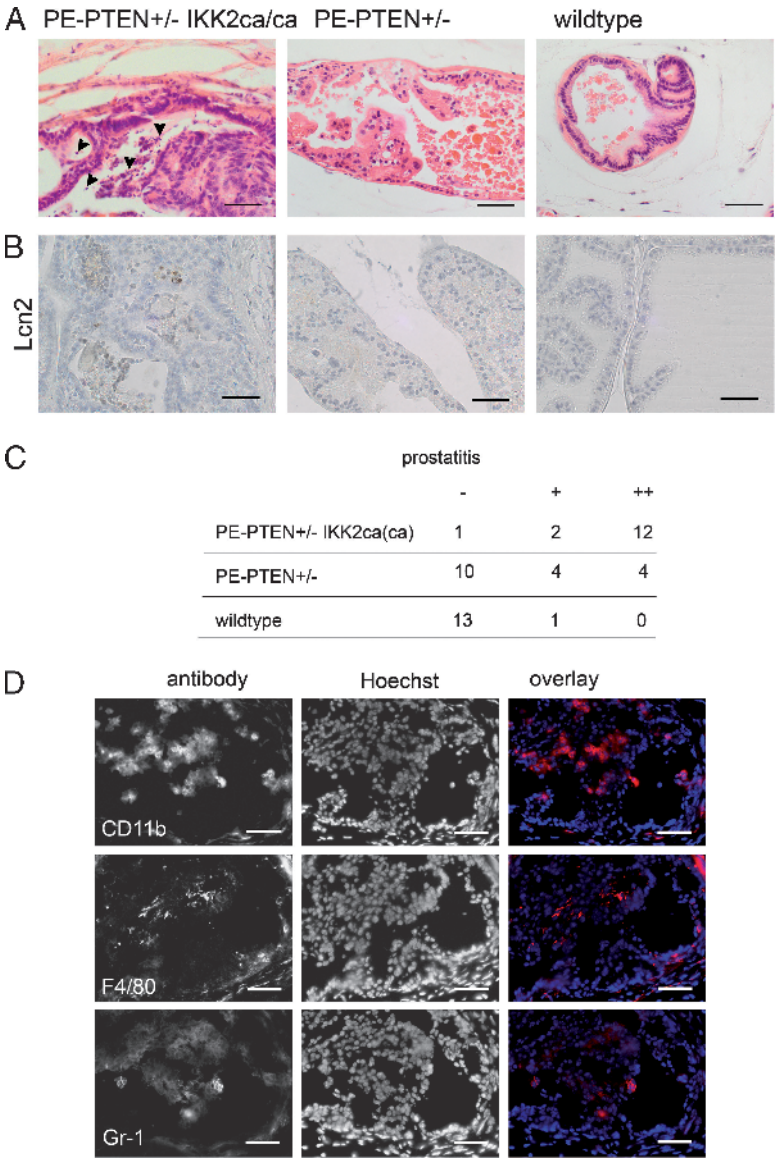

Figure 3. Inflammation in PE−PTEN+/−IKK2ca transgenic prostates. (A) H&E staining of lateral prostates from 12-month-old mice. Arrowheads indicate polymorphonuclear granulocytes. (B) Staining for the neutrophil marker Lipocalin2 (12 months). (C) Analysis of prostatitis seen in transgenic or wild-type prostates at 12 months. − indicates no prostatitis; +, focal prostatitis; ++, prostatitis in the major part of the prostate gland. (D) Antibody staining of consecutive cryosections from dorsal prostates of PE−PTEN+/−IKK2ca/ca mice using marker genes *CD11b*, *F4/80*, and *Gr-1*. Scale bars, 50 μm.

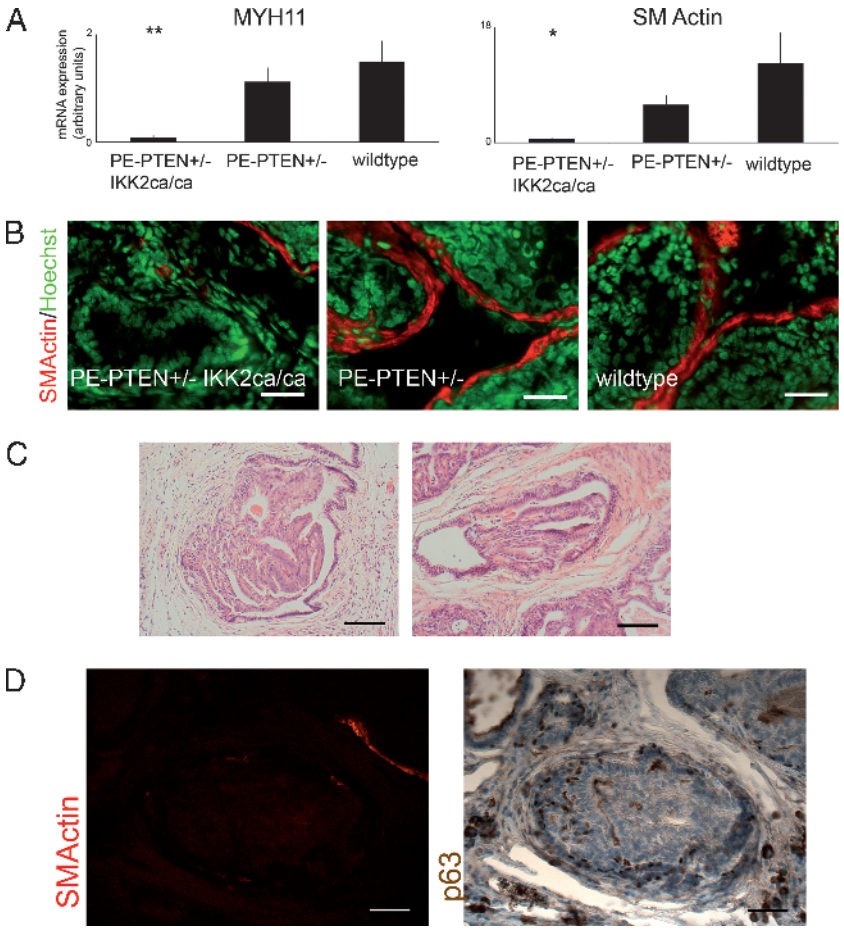

Figure 4. Loss of smooth muscle cells, but no invasion in PE−PTEN+/− IKK2ca(ca) prostates. (A) Quantitative RT-PCR for smooth muscle cell markers from lateral prostates (12 months), $n = 6$ per group. (B) Colored immunofluorescence staining for smooth muscle actin (SM Actin) and Hoechst counterstain in dorsal prostates (12 months). (C) H&E staining of paraffin sections from PE−PTEN+/− IKK2ca/ca prostates. (D) Costaining for SMA and basal cell marker p63 in paraffin-embedded sections from PE−PTEN+/− IKK2ca/ca prostates (12 months). Scale bars, 50 μm (B, D); 100 μm (C). Error bars, SEM. *$P < .05$, **$P < .01$.

actin (*SMA*) in PE–PTEN+/– IKK2ca prostates compared with wild-type or PE–PTEN+/– (Figure 4*A*). This was confirmed by staining lateral prostates with SMA antibody, demonstrating a complete loss of smooth muscle cells around many prostatic ducts (Figure 4*B*). In many tumor models, loss of smooth muscle around the stratified epithelium is indicative of an invasive phenotype. Thus, we reinvestigated our samples for invasive carcinoma formation. Histologically, the larger tumors in PE–PTEN+/– IKK2ca(ca) prostates were still well confined, with no signs of "dripping-off" of smaller epithelial structures or even invasion into the neighboring tissue (Figure 4*C*). Another indication of invasiveness is loss of basal cells in the epithelium. Costaining of smooth muscle marker and the basal cell marker p63 confirmed that, even in glands with complete loss of smooth muscle, basal cell expression is maintained (Figure 4*D*).

Rarely observed carcinomas formed unilaterally in PE–PTEN+/– IKK2ca(ca) prostates, suggestive of a further mutation or transforming event. We examined such a carcinoma and did not find overexpression of factors known to be associated with invasiveness such as *Spink* genes, *Ets* transcription factors, or *myc*, indicating that a different set of genes was responsible for invasiveness (Figure W3).

Taken together, these data show that PE– PTEN+/– IKK2ca prostates exhibit a profound change in the stroma highlighted by a loss of smooth muscle around the stratified epithelium but without regular formation of invasive structures.

Expression Profiling Details the Inflammatory Tumor Phenotype

To gain insight into the molecular mechanism of inflammation and tumor development in the transgenic prostates, we performed microarray analysis on PE–PTEN+/–IKK2ca/ca or PE–PTEN+/– lateral prostates. Overexpressed (PE–PTEN+/– IKK2ca/ca *vs* PE–PTEN+/–) or downregulated genes were determined and grouped according to function (Table 1; the 100 most overexpressed and downregulated genes are listed in Tables W3 and W4). We then confirmed misexpression of many of these genes by quantitative RT-PCR or immunoblot analysis (Figure 5). Consistent with the absence of a histologic phenotype, PE–IKK2ca prostates did not overexpress these candidate genes (Figure W4). One group of genes overexpressed in PE–PTEN+/–IKK2ca/ca prostates constituted chemokines such as *CXCL5*, *CXCL15*, *CCL3*, *CXCL10*, and *CXCL2*. These chemokines are known to attract immune cells, particularly neutrophil granulocytes and monocytes/macrophages, the cells found in the inflamed tissue (Figure 3). Consistently, another group of genes comprised genes found predominantly or exclusively in granulocytes or macrophages. Inflammatory cytokines,

Table 1. Selected Genes from the 100 Most Overexpressed or Underexpressed Genes from Microarray Analysis.

Gene (Abbreviation)	Full Name	Fold Expression
Upregulated genes		
Immune cell associated		
Cd14	Cd14 antigen	6.97
Csf3r	Colony-stimulating factor 3 receptor (granulocyte)	4.83
Mpeg1	Macrophage expressed gene 1	3.64
Chemokines and receptors		
Cxcl5	Chemokine (C-X-C motif) ligand 5	11.68
Cxcl15	Chemokine (C-X-C motif) ligand 15	7.22
Cxcl10	Chemokine (C-X-C motif) ligand 10	5.35
Cxcl2	Chemokine (C-X-C motif) ligand 2	4.10
Ccl3	Chemokine (C-C motif) ligand 3	5.11
Cxcr4	Chemokine (C-X-C motif) receptor 4	3.60
Cytokines and receptors		
Tnf	Tumor necrosis factor	4.28
Il1f9	Interleukin 1 family, member 9	3.85
Il1b	Interleukin 1β	3.62
Il8rb	Interleukin 8 receptor, β	5.15
NF-κB target genes		
C3	Complement component 3	
Nfkbia	IκBα	3.52
Nfkbie	IκBε	4.38
Icam1	Intercellular adhesion molecule 1	6.94
Other		
Sfrp4	Secreted frizzle-related protein 4	7.76
Sfrp1	Secreted frizzle-related protein 1	3.54
Downregulated genes		
Smooth muscle cell markers		
Myh11	Myosin, heavy polypeptide 11, smooth muscle	0.12
Cnn1	Calponin 1	0.18
Spink genes		
Spink3	Serine peptidase inhibitor, Kazal type 3	0.005
Spink5	Serine peptidase inhibitor, Kazal type 5	0.03
Spink11	Serine peptidase inhibitor, Kazal type 11	0.16
Spink8	Serine peptidase inhibitor, Kazal type 8	0.20
Prostate-specific genes		
Pbsn	Probasin	0.06
Tgm4	Transglutaminase 4 (prostate)	0.07
Nkx3-1	NK-3 transcription factor, locus 1 (*Drosophila*)	0.13

RNA was extracted from 12-month-old PE–PTEN+/–IKK2ca/ca or PE–PTEN+/– lateral prostates.

particularly *TNF* but also *IL-1b*, were also overexpressed in the tissues exhibiting prostatitis. These cytokines are known target genes of the transcription factor NF-κB. Other classic NF-κB targets identified included IκB proteins and the adhesion molecule *ICAM1*. Of note, we also identified the secreted frizzle-related proteins 1 and 4 (*SFRP1* and *4*) as overexpressed in PE–PTEN+/–IKK2ca/ca. *SFRP1* has been described as a candidate gene expressed by the stroma to modulate the epithelium in prostate cancer progression [21]. This shows that the activated stroma in our intraepithelial tumors bears resemblance to human prostate cancer stroma.

In line with the analysis of the changes in stroma (Figure 4), some of the most downregulated genes were identified to be smooth muscle cell markers myosin heavy chain 11 (*MYH11*) and calponin 1. Moreover, we found genes associated with prostate tumor progression to be changed: First, the tumor suppressor *Nkx3-1* was downregulated. Nkx3-1 is known to be frequently lost in human prostate cancer, and genetic ablation of the gene in the mouse resulted in hyperplasia and PIN formation [22]. This correlates with our finding of increased tumor proliferation in PE–PTEN+/–IKK2ca and is consistent with findings in a model of bacterial prostatitis [23]. Second, a group of serine protease inhibitors (Spink genes) was downregulated. *Spink3*, which topped the list of downregulated genes, is the murine homolog of human *Spink1*, identified as an upregulated gene in a subset of prostate cancers negative for translocation of Ets transcription factors. In these cancers, *Spink1* overexpression is associated with invasiveness [24]. This correlates with our finding that the larger tumors in PE–PTEN+/–IKK2ca(ca) prostates failed to become invasive carcinomas. Furthermore, the consistent down-regulation of many Spink family members suggests a common regulatory mechanism for Spink genes.

The loss of smooth muscle was also analyzed in human prostate tumors. We used Oncomine (Compendia Bioscience), a database comprising a number of microarray data sets from human tumors, to determine regulation of the markers found in our transgenic mouse lines. We found a number of data sets with down-regulation of smooth muscle cell markers in carcinomas *versus* normal prostate indicating loss of smooth muscle as an event in carcinoma formation (one data set [25] is shown in Figure 5*C*). This confirms that tumors in the inflamed mouse prostate tissue show advanced tumor formation and share similarities with human cancers.

Epithelial and Stromal Cells Produce Inflammatory Chemokines

The inflammatory phenotype in PE–PTEN+/–IKK2ca/ca prostates is somehow evoked by the transgenically modified epithelium. We wanted to confirm that inflammatory chemokines or cytokines overexpressed in the whole prostate tissue samples are indeed produced by the transgenic epithelium. To this end, we established cell lines from transgenic mice and wild-type littermates by explant cultures (Figure 6*A*). Epithelial lines from PE–PTEN+/–IKKca/ca and wild-type prostates expressed E-cadherin and luminal cell marker cytokeratin 18, whereas stromal lines expressed collagen I (Figure W5). Interestingly, a wild-type epithelial (wt) and one transgenic epithelial line (epII) expressed basal cytokeratin 14, whereas another transgenic epithelial line (epI) did not. We conclude that the lines wt and epII show a more intermediate and that the line epI shows a more luminal phenotype based on cytokeratin expression. The Flag-IKK2 transgene was confirmed to be expressed in transgenic epithelium only. *SFRP1*, the reported stroma-to-epithelial modulator, was expressed in the stroma (Figure W5*B*). With respect to chemokine expression, we could show that most of the chemokines are indeed overexpressed in the transgenic epithelium, and their expression was higher in the luminal line compared with the intermediate line (Figure 6). *CXCL5* and *CXCL15* (Figure 6*B*) are strongly overexpressed in the epithelial lines, with moderate overexpression of *CXCL10* and *CXCL2* (not shown). Interestingly, the adhesion molecule *ICAM1* is also strongly overexpressed in the epithelium (Figure 6*B*), and ICAM1 has been described as a receptor for neutrophil granulocytes [26]. This correlates with the finding that these inflammatory cells are located within the epithelium of PE–PTEN+/–IKK2ca/ca prostates (Figure 3). Overexpression of ICAM1 in the epithelium was confirmed by tissue section staining, indicating that it was no cell culture artifact (Figure 6*C*). Moreover, *TNF* was expressed in the transgenic epithelium. We tested the hypothesis that the stroma activated by cytokines from the epithelium could also express immune cell-attracting chemokines. Indeed, TNF treatment of stromal cultures induced messenger RNA (mRNA) of *CXCL2* (Figure 6*D*) and, to a lesser extent, *CXCL10* (Figure W5) but not *CXCL5* or *CXCL15*. Furthermore, treatment of the epI cell line with the IKK/NF-κB inhibitor BMS-345541 decreased cytokine and chemokine expression, confirming that the transgenic activation of the IKK2/NF-κB axis is responsible for the overexpression of these molecules (Figure 6*E*).

Taken together, these data indicate that the transgenic PTEN+/–IKK2ca/ca epithelium can attract inflammatory cells by direct and/or indirect production of chemokines.

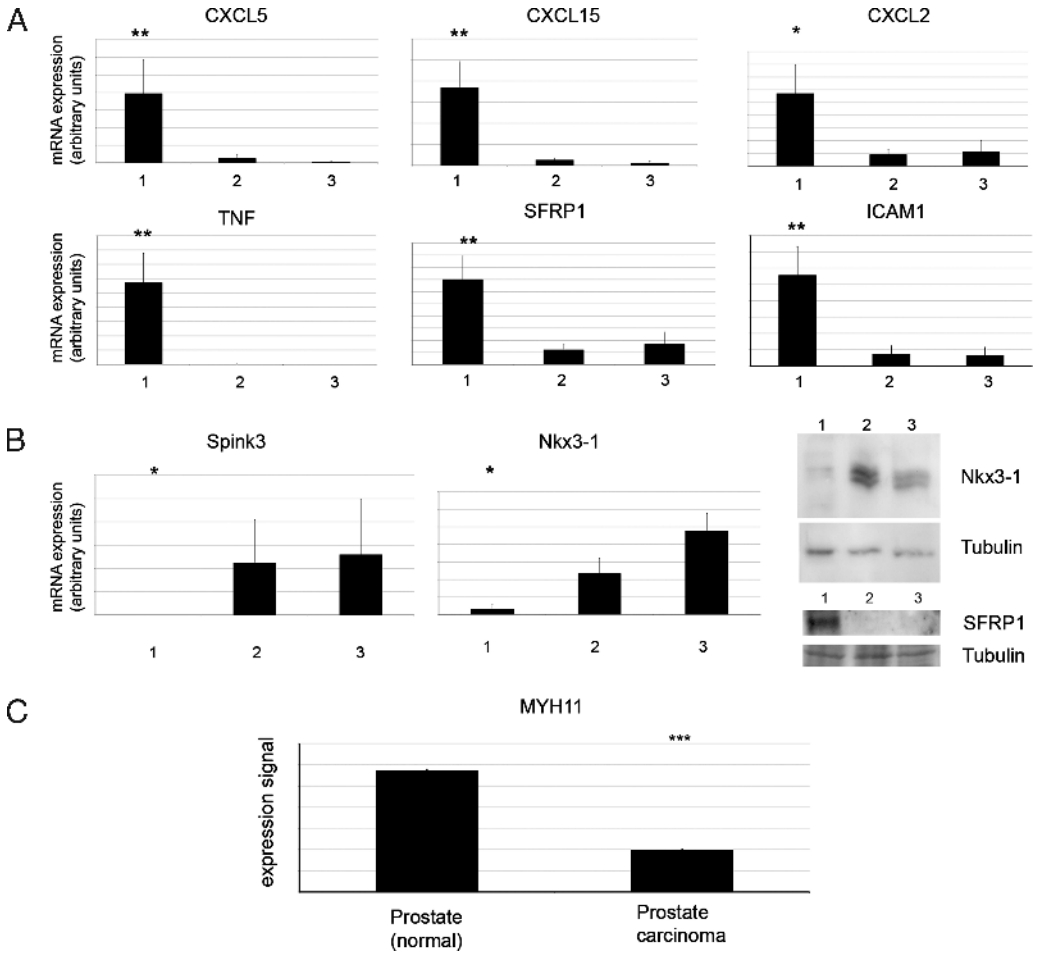

Figure 5. Confirmation of gene expression changes in transgenic prostates. (A, B) Quantitative RT-PCR experiments on samples from PE−PTEN+/−IKK2ca/ca prostates (group 1), PE−PTEN+/− prostates (group 2), and wild-type littermate controls (group 3) ($n = 6$ per group, extracted from 12-month-old tissues). (B) Immunoblot for Nkx3-1 and SFRP-1 (right panel). (C) Data mining of normal prostate *versus* human prostate cancer. The data set of Vanaja et al. was queried by use of Oncomine, and the expression data were transformed to the linear expression signal plotted in the bar graph. Error bars, SEM. *$P < .05$; **$P < .01$; ***$P < .001$.

Loss of Smooth Muscle Correlates with Prostate Inflammation

We wanted to establish a correlation between the inflammatory phenotype and loss of smooth muscle. To this end, we stained PE–PTEN+/– IKK2ca/ca dorsal prostates where smooth muscle was only partially lost, with both smooth muscle (SMA) and inflammatory cell marker (CD11b). In prostatic ducts with intense inflammatory cell infiltration, the smooth muscle was lost completely (Figure 7*A*, *arrow*), whereas in ducts with little or no signs of inflammation, the smooth muscle was maintained or partially intact (Figure 7*A*, *arrowheads*). Quantification over a number of prostatic ducts established a correlation between smooth muscle thickness and inflammatory cell infiltration (Figure 7*B*).

Reduced Epithelial Androgen Receptor Activation in Transgenic Prostates

Down-regulation of *Nkx3-1*, an androgen-responsive gene, in PE–PTEN+/–IKK2ca prostates suggested reduced AR activation in the epithelium. Staining of wild-type and transgenic prostates showed less nuclear (activated) AR in the hyperplastic tissues (Figure 8, *A* and *B*). A decrease in AR activity was also indicated by down-regulation of other androgen-responsive genes such as *Probasin* (Figure 8*C*). These data suggest that decreased AR activity could be responsible for the hyperplastic epithelium by downregulating Nkx3-1.

Discussion

In this study, we sought to elucidate the effects of inflammation and inflammatory signaling on early events of prostate tumorigenesis. The main reason for this is that epidemiological data suggest a role for inflammation in tumor initiation or early progression. Thus, we analyzed IKK2 signaling on a wild-type and PE–PTEN+/–, but not PE–PTEN–/– background, because the latter has been described to result in full carcinoma formation over time. The effect of NF-κB signaling on late-stage prostate tumorigenesis has been addressed by other groups and determined a role for NF-κB in promoting androgen-independent growth [27].

Inflammatory signaling through constitutive activation of the IKK2 axis in normal prostate epithelium is insufficient to transform prostate tissue. This is interesting because IKK2 has been shown to be an oncogenic kinase and activation on a PE–PTEN+/– background shows a clear additional phenotype. One possible reason for this lack of phenotype may be that IKK2/NF-κB transcription factors can activate promoters in proliferating epithelium that they cannot activate in

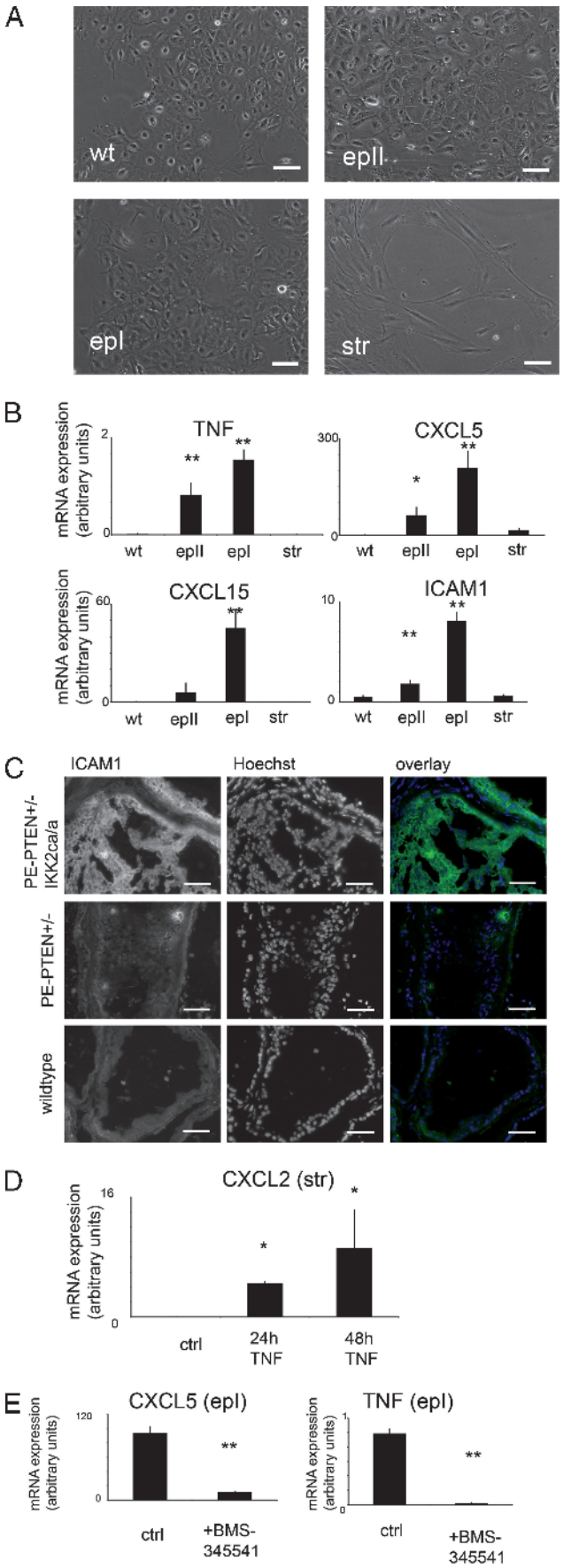

quiescent epithelium such as the prostate epithelium. Consistent with this, some NF-κB dependent promoters were not activated in PE–IKK2ca prostates compared with wild-type prostates. Moreover, we have found a clear phenotype- and NF-κB–dependent gene expression when expressing the same transgene from the same strain in keratinocytes of the skin, a proliferating epithelium (Birbach et al., unpublished observations). The Probasin-Cre strain used in our study excises loxP-flanked sequences only in the adult, quiescent epithelium. Excision efficiency increases with age, in line with the age-dependent phenotype in PE–PTEN+/–IKK2ca(ca) [28].

Our experiments on PE–PTEN+/–IKK2ca(ca) indicate that some of the more upregulated genes in prostate epithelium in response to NF-κB are inflammatory cytokines and chemokines. This is in agreement with chemokine production from other epithelia in response to NF-κB [29]. The chemokines from the epithelium and cytokine-activated stroma (a finding consistent with data from human stromal cells [30]) are likely attractors for the infiltrating inflammatory cells. The inflammation evoked phenotype in both the epithelium and the stroma: the severe hyperplasia in dysplastic epithelial lesions was due to the increased proliferation, not apoptosis, consistent with expression data indicating no major change in regulators of apoptosis, but down-regulation of Nkx3-1, a guardian of epithelial proliferation. Nkx3-1 loss in the epithelium is necessary for tumor initiation in tumor models and human cancer and could have a similar function in our model [31]. Reduced AR activation is a likely contributor to the decrease in Nkx3-1. In this context, the relationship between NF-κB and AR activity is complex, with different outcomes in *in vitro* experiments by different groups [32,33]. In our model, we hypothesize that the modified stromal-to-epithelial signaling could play a role in modifying AR activity.

In the stroma, increases in fibroblasts and collagen fibers were reminiscent of activated prostate cancer stroma, and expression data showed some upregulated genes known for their expression in cancer-associated fibroblasts. Loss of smooth muscle and concomitant increase of stromal fibroblasts suggest that the smooth muscle is lost by a dedifferentiation to fibroblastic cells. Various factors have been described to be involved in smooth muscle dedifferentiation, including inflammatory mediators [34,35]. Prostate smooth muscle cells can be partially dedifferentiated by LPS treatment, and partial vascular smooth muscle dedifferentiation by IL-1b can be enhanced by PGE-2. Along the same lines, we have observed a small decrease in smooth muscle markers by treating prostate stroma with TNF (not shown). Although neither of these experiments (during a time span of hours to days) result in complete loss of smooth muscle identity, it is conceivable that persistent inflammation for months and possible additive effects of different inflammatory mediators can lead to complete dedifferentiation.

Figure 6. Inflammatory cytokines and chemokines are expressed in cultured epithelial and stromal cells. (A) Bright-field images from cell cultures of prostate epithelial cells from nontransgenic prostates (wt) or PE− PTEN+/− IKK2ca/ca prostates (epI, epII) and from cultures of prostate stromal cells from PE−PTEN+/− IKK2ca/ca prostates (str). (B) Quantitative RT-PCR data ($n = 3$ per group). (C) Immunostaining for ICAM1 in frozen sections of dorsal prostates (12 months) of the indicated genotypes. (D) Chemokine CXCL2 mRNA was determined in cultured stromal cells with or without TNF treatment for 24 or 48 hours (ctrl: untreated control). (E) mRNA was determined in epI epithelial line treated with mock control or BMS-345541 for 72 hours. Scale bars, 50 μm. Error bars, SEM. *$P < .05$; **$P < .01$.

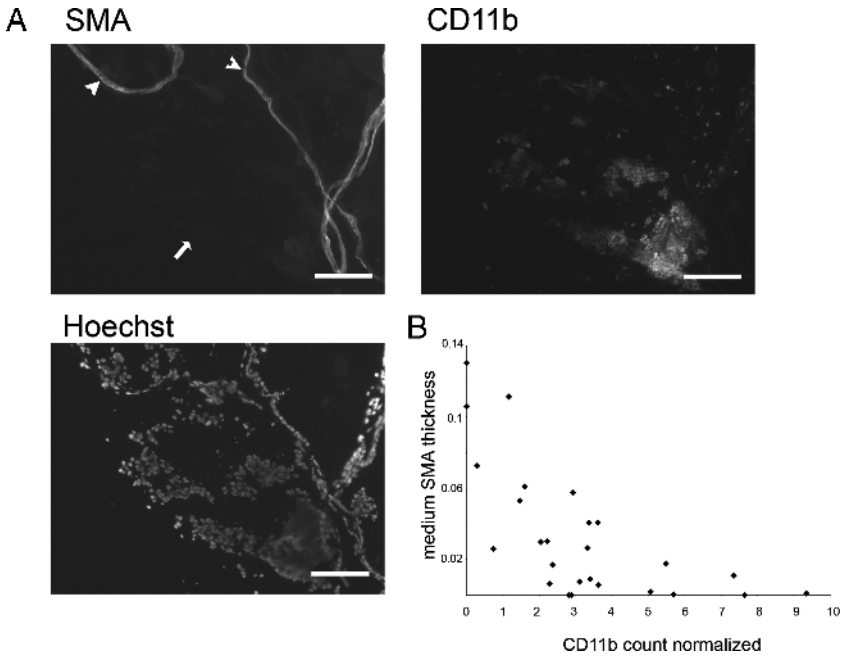

Figure 7. Correlation of inflammatory cell infiltration and smooth muscle thickness. (A) Cryosections from 11-month-old PTEN+/−IKK2ca/ca dorsal prostate were stained as indicated. Arrow indicates duct with loss of smooth muscle and infiltration of inflammatory cells. Arrowheads indicate ducts still surrounded by smooth muscle and less infiltration. (B) Quantification of dorsal prostate ducts (8-12 months). Scale bars, 100 μm.

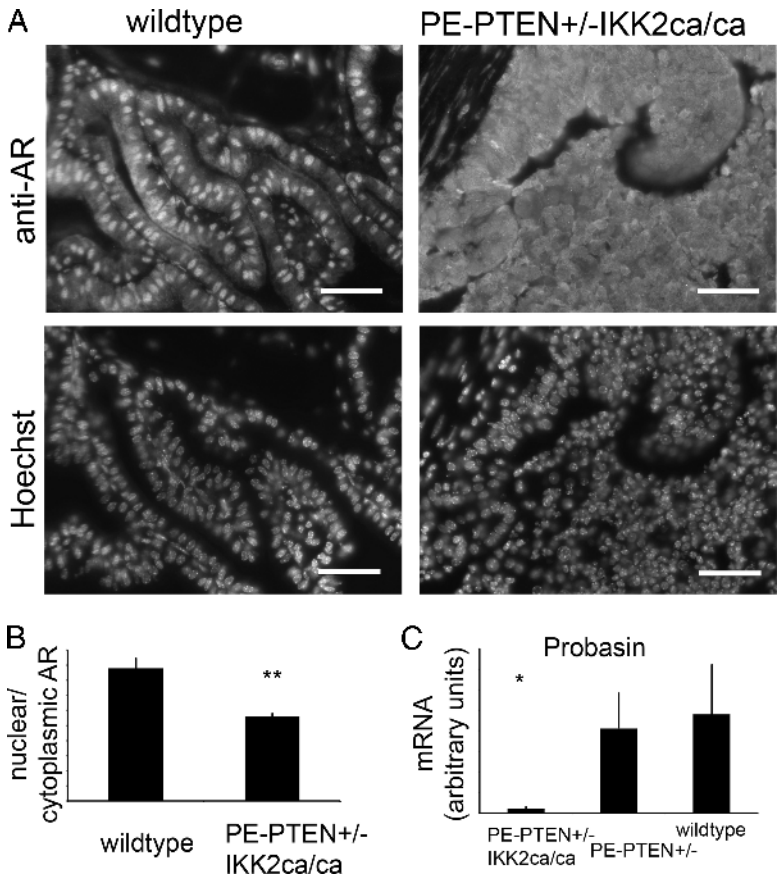

Figure 8. Reduced epithelial AR activation in PE−PTEN+/−IKK2ca/ca. (A) Paraffin sections of wild-type and transgenic tissue (anterior prostate, 12 months) stained for AR with Hoechst counterstain. (B) Quantification for wild-type and transgenic tissues ($n = 4$ each). (C) Quantitative PCR of androgen-responsive gene *Probasin* ($n = 6$ per group). Scale bars, 50 μm. $^{**}P < .01$; $^{*}P < .05$.

Although the smooth muscle around the prostatic ducts was lost, most tumors were not invasive by histologic or expression parameters. We laid emphasis on maintaining our mouse colony on a strict C57BL/6 background, known as a strain with low tumor susceptibility [36]. It is well possible that more carcinomas, especially microinvasive structures, develop on a different inbred or mixed background; however, by using this approach, we were able to clearly distinguish the effects mediated by the inflammatory phenotype from the secondary events dependent on another genetic or epigenetic alteration in the tumor. Along these lines, tumor models with partial loss of Nkx3-1 on a PE–PTEN+/– background have been shown to be more frequently invasive than the tumors in our study but were bred on a mixed background [37].

Loss of smooth muscle has been used as a hallmark for carcinoma formation in mouse prostate tumor models [16,38]. Models of epithelial-stromal interactions have proposed smooth muscle integrity to be necessary to control epithelial proliferation and dysplasia [39,40]. Moreover, human prostate carcinoma is associated with downregulation of smooth muscle markers. Our data from the inflammatory model show that loss of smooth muscle is not sufficient for the tumor to become invasive but that the two events can be uncoupled.

One model of prostate carcinogenesis based on genetic analysis and mouse models of prostate tumors suggests that a distinct step associated with the overexpression of either Ets transcription factors, *Spink1* gene, or other, yet unidentified genes must be taken to induce invasion through the basement membrane and carcinoma formation [24,41]. This is in agreement with our expression data from intraepithelial tumors of inflamed prostates with either unchanged (Ets factors) or even downregulated (*Spink* genes) invasion-associated genes.

In summary, as a genetic model, our model has advantages over bacterially induced models of inflammatory tumorigenesis. It is a reproducible model based on well-defined Cre-mediated deletion and dissects effects mediated by inflammation and genetic lesions. Inflamed prostates not only show enlarged tumor burden due to increased proliferation but also exhibit a clear change in stromal mass and composition. On a well-defined background, the model demonstrates what inflammation does by its own and what is due to genetic background or further genetic or epigenetic alterations in the tumor. Invasion, although rarely seen in our model, will be present in inflammatory tumors but is not a direct consequence of inflammation in our model. Loss of smooth muscle, an indicator of tumor progression, is seen in inflammatory lesions and correlates with inflammation. Interestingly, genetic data have revealed that loss of smooth muscle markers in primary tumors is part of a tumor signature predicting subsequent metastasis and poor clinical outcome [42]. Thus, the inflammatory tumors in our model, although not invasive without a subsequent transforming step, may be more dangerous in the long run when acquiring additional mutations to become carcinomas.

Acknowledgments

The authors thank Tak Mak for the loxP-PTEN mice, Gernot Schabbauer for sharing mice from his cohort, and Renate Kain for help with tissue processing for histology.

References

[1] Kuper H, Adami HO, and Trichopoulos D (2000). Infections as a major preventable cause of human cancer. *J Intern Med* **248**, 171–183.

[2] Grivennikov SI, Greten FR, and Karin M (2010). Immunity, inflammation, and cancer. *Cell* **140**, 883–899.

[3] De Marzo AM, Platz EA, Sutcliffe S, Xu J, Gronberg H, Drake CG, Nakai Y, Isaacs WB, and Nelson WG (2007). Inflammation in prostate carcinogenesis. *Nat Rev Cancer* **7**, 256–269.

[4] MacLennan GT, Eisenberg R, Fleshman RL, Taylor JM, Fu P, Resnick MI, and Gupta S (2006). The influence of chronic inflammation in prostatic carcinogenesis: a 5-year followup study. *J Urol* **176**, 1012–1016.

[5] Mahmud S, Franco E, and Aprikian A (2004). Prostate cancer and use of nonsteroidal anti-inflammatory drugs: systematic review and meta-analysis. *Br J Cancer* **90**, 93–99.

[6] Dennis LK, Lynch CF, and Torner JC (2002). Epidemiologic association between prostatitis and prostate cancer. *Urology* **60**, 78–83.

[7] Putzi MJ and De Marzo AM (2000). Morphologic transitions between proliferative inflammatory atrophy and high-grade prostatic intraepithelial neoplasia. *Urology* **56**, 828–832.

[8] Quintar AA, Doll A, Leimgruber C, Palmeri CM, Roth FD, Maccioni M, and Maldonado CA (2010). Acute inflammation promotes early cellular stimulation of the epithelial and stromal compartments of the rat prostate. *Prostate* **70**, 1153–1165.

[9] Elkahwaji JE, Hauke RJ, and Brawner CM (2009). Chronic bacterial inflammation induces prostatic intraepithelial neoplasia in mouse prostate. *Br J Cancer* **101**, 1740–1748.

[10] Schmid JA and Birbach A (2008). IκB kinase beta (IKKβ/IKK2/IKBKB)—a key molecule in signaling to the transcription factor NF-κB. *Cytokine Growth Factor Rev* **19**, 157–165.

[11] Lee DF, Kuo HP, Chen CT, Hsu JM, Chou CK, Wei Y, Sun HL, Li LY, Ping B, Huang WC, et al. (2007). IKKβ suppression of TSC1 links inflammation and tumor angiogenesis via the mTOR pathway. *Cell* **130**, 440–455.

[12] Lee DF, Kuo HP, Liu M, Chou CK, Xia W, Du Y, Shen J, Chen CT, Huo L, Hsu MC, et al. (2009). KEAP1 E3 ligase–mediated downregulation of NF-κB signaling by targeting IKKβ. *Mol Cell* **36**, 131–140.

[13] Wu X, Wu J, Huang J, Powell WC, Zhang J, Matusik RJ, Sangiorgi FO, Maxson RE, Sucov HM, and Roy-Burman P (2001). Generation of a prostate epithelial cell–specific Cre transgenic mouse model for tissue-specific gene ablation. *Mech Dev* **101**, 61–69.

[14] Trotman LC, Niki M, Dotan ZA, Koutcher JA, Di Cristofano A, Xiao A, Khoo AS, Roy-Burman P, Greenberg NM, Van Dyke T, et al. (2003). Pten dose dictates cancer progression in the prostate. *PLoS Biol* **1**, E59.

[15] Ma X, Ziel-van der Made AC, Autar B, van der Korput HA, Vermeij M, van Duijn P, Cleutjens KB, de Krijger R, Krimpenfort P, Berns A, et al. (2005). Targeted biallelic inactivation of Pten in the mouse prostate leads to prostate cancer accompanied by increased epithelial cell proliferation but not by reduced apoptosis. *Cancer Res* **65**, 5730–5739.

[16] Wang S, Gao J, Lei Q, Rozengurt N, Pritchard C, Jiao J, Thomas GV, Li G, Roy-Burman P, Nelson PS, et al. (2003). Prostate-specific deletion of the murine Pten tumor suppressor gene leads to metastatic prostate cancer. *Cancer Cell* **4**, 209–221.

[17] Suzuki A, Yamaguchi MT, Ohteki T, Sasaki T, Kaisho T, Kimura Y, Yoshida R, Wakeham A, Higuchi T, Fukumoto M, et al. (2001). T cell–specific loss of Pten leads to defects in central and peripheral tolerance. *Immunity* **14**, 523–534.

[18] Sasaki Y, Derudder E, Hobeika E, Pelanda R, Reth M, Rajewsky K, and Schmidt-Supprian M (2006). Canonical NF-κB activity, dispensable for B cell development, replaces BAFF-receptor signals and promotes B cell proliferation upon activation. *Immunity* **24**, 729–739.

[19] Barclay WW and Cramer SD (2005). Culture of mouse prostatic epithelial cells from genetically engineered mice. *Prostate* **63**, 291–298.

[20] Birbach A, Casanova E, and Schmid JA (2009). A Probasin-MerCreMer BAC allows inducible recombination in the mouse prostate. *Genesis* **47**, 757–764.

[21] Joesting MS, Perrin S, Elenbaas B, Fawell SE, Rubin JS, Franco OE, Hayward SW, Cunha GR, and Marker PC (2005). Identification of SFRP1 as a candidate mediator of stromal-to-epithelial signaling in prostate cancer. *Cancer Res* **65**, 10423–10430.

[22] Kim MJ, Bhatia-Gaur R, Banach-Petrosky WA, Desai N, Wang Y, Hayward SW, Cunha GR, Cardiff RD, Shen MM, and Abate-Shen C (2002). Nkx3.1 mutant mice recapitulate early stages of prostate carcinogenesis. *Cancer Res* **62**, 2999–3004.

[23] Khalili M, Mutton LN, Gurel B, Hicks JL, De Marzo AM, and Bieberich CJ (2010). Loss of Nkx3.1 expression in bacterial prostatitis: a potential link between inflammation and neoplasia. *Am J Pathol* **176**, 2259–2268.

[24] Tomlins SA, Rhodes DR, Yu J, Varambally S, Mehra R, Perner S, Demichelis F, Helgeson BE, Laxman B, Morris DS, et al. (2008). The role of SPINK1 in ETS rearrangement-negative prostate cancers. *Cancer Cell* **13**, 519–528.

[25] Vanaja DK, Cheville JC, Iturria SJ, and Young CY (2003). Transcriptional silencing of zinc finger protein 185 identified by expression profiling is associated with prostate cancer progression. *Cancer Res* **63**, 3877–3882.

[26] Diamond MS, Staunton DE, de Fougerolles AR, Stacker SA, Garcia-Aguilar J, Hibbs ML, and Springer TA (1990). ICAM-1 (CD54): a counter-receptor for Mac-1 (CD11b/CD18). *J Cell Biol* **111**, 3129–3139.

[27] Jin RJ, Lho Y, Connelly L, Wang Y, Yu X, Saint Jean L, Case TC, Ellwood-Yen K, Sawyers CL, Bhowmick NA, et al. (2008). The nuclear factor-κB pathway controls the progression of prostate cancer to androgen-independent growth. *Cancer Res* **68**, 6762–6769.

[28] Roy-Burman P, Wu H, Powell WC, Hagenkord J, and Cohen MB (2004). Genetically defined mouse models that mimic natural aspects of human prostate cancer development. *Endocr Relat Cancer* **11**, 225–254.

[29] Richmond A (2002). Nf-κB, chemokine gene transcription and tumour growth. *Nat Rev Immunol* **2**, 664–674.

[30] Kogan-Sakin I, Cohen M, Paland N, Madar S, Solomon H, Molchadsky A, Brosh R, Buganim Y, Goldfinger N, Klocker H, et al. (2009). Prostate stromal cells produce CXCL-1, CXCL-2, CXCL-3 and IL-8 in response to epithelia-secreted IL-1. *Carcinogenesis* **30**, 698–705.

[31] Lei Q, Jiao J, Xin L, Chang CJ, Wang S, Gao J, Gleave ME, Witte ON, Liu X, and Wu H (2006). NKX3.1 stabilizes p53, inhibits AKT activation, and blocks prostate cancer initiation caused by PTEN loss. *Cancer Cell* **9**, 367–378.

[32] Supakar PC, Jung MH, Song CS, Chatterjee B, and Roy AK (1995). Nuclear factor κB functions as a negative regulator for the rat androgen receptor gene and NF-κB activity increases during the age-dependent desensitization of the liver. *J Biol Chem* **270**, 837–842.

[33] Delfino FJ, Boustead JN, Fix C, and Walker WH (2003). NF-κB and TNF-α stimulate androgen receptor expression in Sertoli cells. *Mol Cell Endocrinol* **201**, 1–12.

[34] Clement N, Glorian M, Raymondjean M, Andreani M, and Limon I (2006). PGE_2 amplifies the effects of IL-1β on vascular smooth muscle cell de-differentiation: a consequence of the versatility of PGE_2 receptors 3 due to the emerging expression of adenylyl cyclase 8. *J Cell Physiol* **208**, 495–505.

[35] Leimgruber C, Quintar AA, Sosa LD, Garcia LN, Figueredo M, and Maldonado CA (2010). Dedifferentiation of prostate smooth muscle cells in response to bacterial LPS. *Prostate* **71**, 1097–1107.

[36] Deschner EE, Long FC, Hakissian M, and Herrmann SL (1983). Differential susceptibility of AKR, C57BL/6J, and CF1 mice to 1,2-dimethylhydrazine–induced colonic tumor formation predicted by proliferative characteristics of colonic epithelial cells. *J Natl Cancer Inst* **70**, 279–282.

[37] Abate-Shen C, Banach-Petrosky WA, Sun X, Economides KD, Desai N, Gregg JP, Borowsky AD, Cardiff RD, and Shen MM (2003). Nkx3.1; Pten mutant mice develop invasive prostate adenocarcinoma and lymph node metastases. *Cancer Res* **63**, 3886–3890.

[38] Wang Y, Hayward SW, Donjacour AA, Young P, Jacks T, Sage J, Dahiya R, Cardiff RD, Day ML, and Cunha GR (2000). Sex hormone–induced carcinogenesis in Rb-deficient prostate tissue. *Cancer Res* **60**, 6008–6017.

[39] Cunha GR, Hayward SW, Dahiya R, and Foster BA (1996). Smooth muscle–epithelial interactions in normal and neoplastic prostatic development. *Acta Anat (Basel)* **155**, 63–72.

[40] Wong YC and Tam NN (2002). Dedifferentiation of stromal smooth muscle as a factor in prostate carcinogenesis. *Differentiation* **70**, 633–645.

[41] Tomlins SA, Laxman B, Varambally S, Cao X, Yu J, Helgeson BE, Cao Q, Prensner JR, Rubin MA, Shah RB, et al. (2008). Role of the *TMPRSS2-ERG* gene fusion in prostate cancer. *Neoplasia* **10**, 177–188.

[42] Ramaswamy S, Ross KN, Lander ES, and Golub TR (2003). A molecular signature of metastasis in primary solid tumors. *Nat Genet* **33**, 49–54.

Table W1. List of Oligonucleotides Used for Quantitative PCR Analysis.

Gene (Symbol) or Amplicon	Primer Sequences (Sense and Antisense, 5′ → 3′)
CXCL2	GCGCCCAGACAGAAGTCATAG
	AGCCTTGCCTTTGTTCAGTATC
CXCL5	GAAAGCTAAGCGGAATGCAC
	GGGACAATGGTTTCCCTTTT
CXCL10	GCTCCTGCATCAGCACCAGC
	CTTGAACGACGACGACTTTGG
CXCL15	CCA TGG GTG AAG GCT ACT GT
	TCT CAG GTC TCC CAA ATG AAA
Cytokeratin18	CAGCCAGCGTCTATGCAGG
	CTTTCTCGGTCTGGATTCCAC
ICAM1	TGC GTT TTG GAG CTA GCG GAC CA
	CGA GGA CCA TAC AGC ACG TGC AG
TNF	TAGCCAGGAGGGAGAACAGA
	TTTTCTGGAGGGAGATGTGG
E-Cadherin	AAGTGACCGATGATGATGCC
	CTTCTCTGTCCATCTCAGCG
Collagen1	CAC CCT CAA GAG CCT GAG TC
	GTT CGG GCT GAT GTA CCA GT
Flag-IKK2	GAC TAC AAG GAC GAC GAT GAC AAG
	GGT TCA GCC TTC TCA TGA TCT GG
SFRP1	CAACGTGGGCTACAAGAAGAT
	GGCCAGTAGAAGCCGAAGAAC
SFRP4	AGAAGGTCCATACAGTGGGAAG
	GTTACTGCGACTGGTGCGA
Nkx3-1	ATGCTTAGGGTAGCGGAGC
	TGCGGATTGCCTGAGTGTC
Spink3	ATG AAG GTG GCT GTC ATC TTT C
	TCA GCA AGG CCC ACC TTT TCG
Smooth muscle actin	GTCCCAGACATCAGGGAGTAA
	TCGGATACTTCAGCGTCAGGA
Probasin	AAGGCTCACCATTGAGAACCT
	CAGTTGGCACTTAGTCCCTTTC
MYH11	AAGCTGCGGCTAGAGGTCA
	CCCTCCCTTTGATGGCTGAG
HPRT	CAA ATC AAA AGT CTG GGG ACG C
	GCT TGC TGG TGA AAA GGA CCT C

Table W2. List of Antibodies Used in This Study.

Antibody/Antigen	Source/Catalog No. (or Equivalent)	Use/Dilution
CD3e	eBioscience/13-0031	IF-F/1:200
F4/80	eBioscience/13-4801	IF-F/1:200
CD11b	eBioscience/13-0112	IF-F/1:200
Gr-1	eBioscience/13-5931	IF-F/1:200
Ki67	Neomarkers/RM-9106-S1	IF-P/1:200
Lipocalin2	Santa Cruz/sc-18698	IHC-P/1:200
Nkx3-1	Santa Cruz/sc-15022	IB/1:400
Smooth muscle actin	Sigma/C6198	IF-P/1:400
		IF-F/1:400
P63	Santa Cruz/sc-56188	IF-P/1:100
Cytokeratin14	Prof E.B. Lane (University of Dundee)	IF-cells/1:10
Androgen receptor	Santa Cruz/sc-815	IF-P/1:100
β-Tubulin	Santa Cruz/sc-9104	IB/1:400
IκBα	Santa Cruz/sc-371	IB/1:1000, IF-F/1:100
ICAM1	eBioscience/14-0541	IF-F/1:100
A555 goat antirabbit	Invitrogen/A-21428	IF-P, IF-F/1:2000
Biotin antirabbit	Vector Laboratories/BA-1000	IHC-P/1:400
Biotin antigoat	Vector Laboratories/BA-9500	IHC-P/1:400
Biotin antimouse	Vector Laboratories/BA-9200	IHC-P/1:400
Streptavidin, Alexa Fluor 555 conjugate	Invitrogen/S32355	IF-F/1:500

F indicates frozen sections; IB, immunoblot; IF, immunofluorescence; IHC, immunohistochemistry; P, paraffin sections.

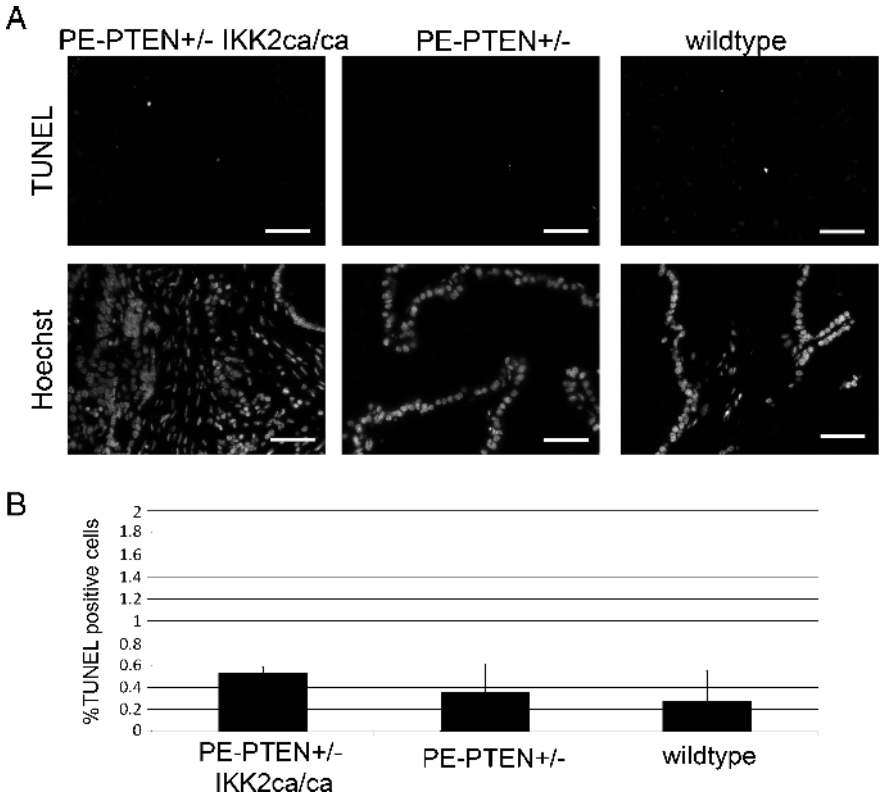

Figure W1. TUNEL stain indicating no change in apoptosis in transgenic *versus* wild-type prostases. (A) TUNEL staining (see Materials and Methods) was performed on paraffin sections from prostates of the indicated genotypes. Hoechst staining is given to indicate tissue architecture and cell density. (B) Quantification of TUNEL-positive cells in lateral cells in the lateral prostates of the indicated genotypes ($n = 4$ per group). Error bars, SEM. No statistical significance was reached in the analysis of variance.

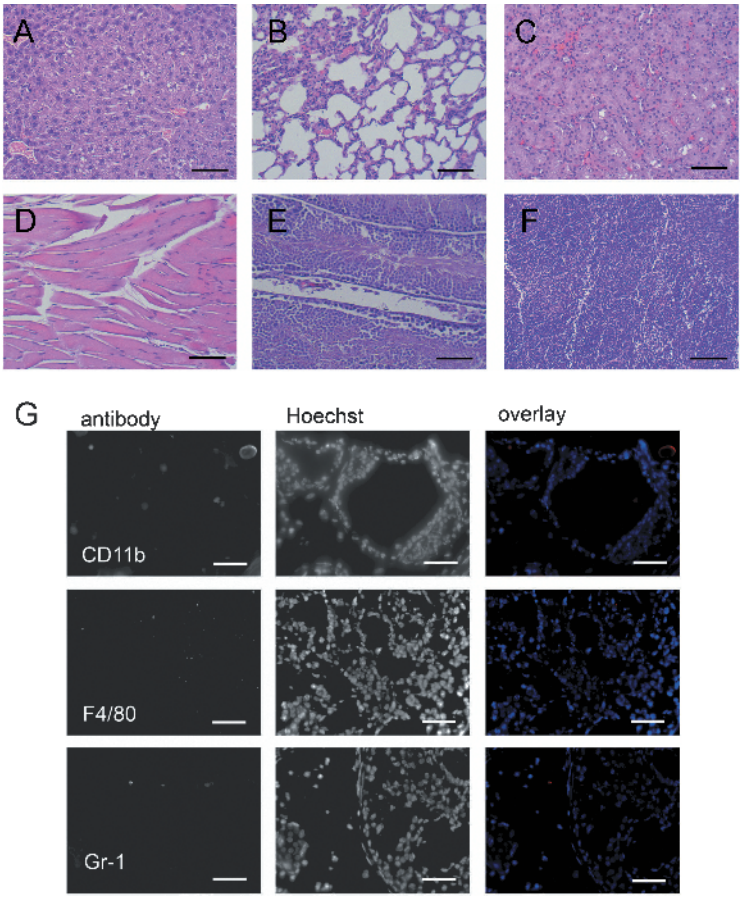

Figure W2. Normal histologic finding of nonprostate tissues from PE−PTEN+/− IKK2ca/ca mice (A-F) and lack of immunoreactivity in PE−PTEN+/− lateral prostates (G). H&E stains are shown for liver (A), lung (B), kidney (C), muscle tissue surrounding the urethra (D), testis (E), and lymph node (F). Scale bars, 100 μm. (G) Antibody staining in PE−PTEN+/− lateral prostates. Scale bars, 50 μm.

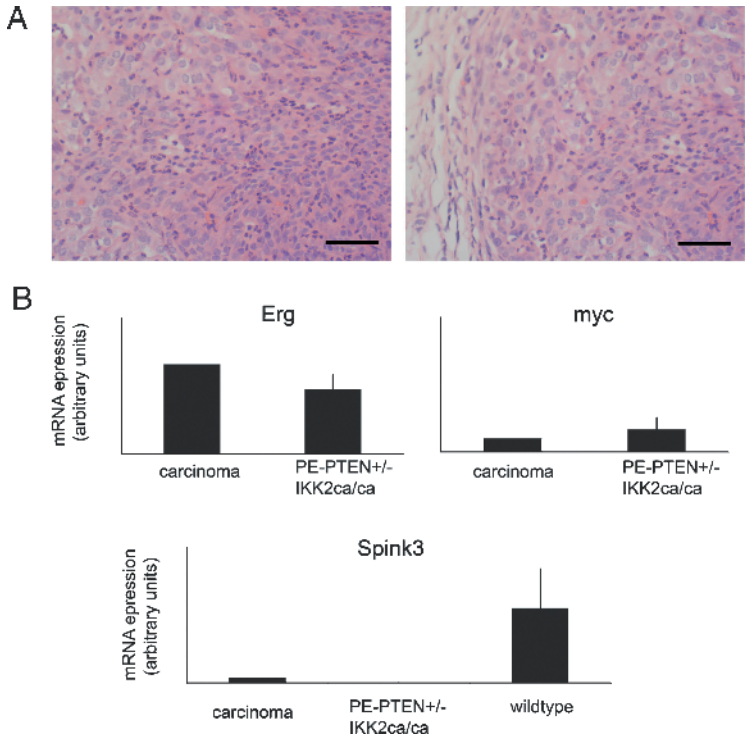

Figure W3. Carcinoma formation in a PTEN+/−IKK2ca/ca lateral prostate (12 months). (A) H&E stain of the tumor itself (left) and adjacent to the stroma (right). (B) Quantitative PCR data of carcinoma ($n = 1$) compared with PE−PTEN+/−IKK2ca/ca prostate ($n = 3$) or wild-type prostate ($n = 3$). Scale bars, 50 μm.

Table W3. The 100 Most Overexpressed Genes in the Microarray Study Comparing PE–PTEN+/–IKK2ca/ca to PE–PTEN+/–.

Gene Symbol	Full Name	Fold Expression
Msln	Mesothelin	33.12
Ly6d	Lymphocyte antigen 6 complex, locus D	13.64
Gabrp	γ-Aminobutyric acid (GABA) A receptor, pi	13.16
Hp	Haptoglobin	11.96
Clca2	Chloride channel calcium activated 2	11.78
Cxcl5	Chemokine (C-X-C motif) ligand 5	11.68
Olfm4	Olfactomedin 4	9.95
Egln3	EGL nine homolog 3 (*C. elegans*)	8.26
Slco1a5	Solute carrier organic anion transporter family, member 1a5	7.98
Sfrp4	Secreted frizzle-related protein 4	7.76
AW112010	Expressed sequence AW112010	7.61
Sftpd	Surfactant associated protein D	7.26
Gdpd3	Glycerophosphodiester phosphodiesterase domain containing 3	7.23
Cxcl15	Chemokine (C-X-C motif) ligand 15	7.22
Ccdc129	Coiled-coil domain containing 129	7.00
Cd14	CD14 antigen	6.97
Icam1	Intercellular adhesion molecule 1	6.94
Tnfsf10	Tumor necrosis factor (ligand) superfamily, member 10	6.90
Car13	Carbonic anhydrase 13	6.90
Muc20	Mucin 20	6.78
Ctla2a	Cytotoxic T-lymphocyte–associated protein 2α	6.66
Atp6v1b1	ATPase, H^+ transporting, lysosomal V1 subunit B1	6.48
Aspa	Aspartoacylase	6.42
C3	Complement component 3	6.07
Ltbp2	Latent transforming growth factor β binding protein 2	5.98
S100a8	S100 calcium binding protein A8 (calgranulin A)	5.74
Car2	Carbonic anhydrase 2	5.57
Cxcl10	Chemokine (C-X-C motif) ligand 10	5.35
Clic6	Chloride intracellular channel 6	5.28
Clip4	CAP-GLY domain containing linker protein family, member 4	5.21
Vsig1	V-set and immunoglobulin domain containing 1	5.20
Wfdc2	WAP four-disulfide core domain 2	5.18
Il8rb	Interleukin 8 receptor, β	5.15
Ccl3	Chemokine (C-C motif) ligand 3	5.11
Ttc9	Tetratricopeptide repeat domain 9	5.05
Cyba	Cytochrome *b*-245, α polypeptide	5.01
Clec4d	C-type lectin domain family 4, member d	4.94
Cp	Ceruloplasmin	4.89
Tnip3	TNFAIP3 interacting protein 3	4.84
Csf3r	Colony stimulating factor 3 receptor (granulocyte)	4.83
Mmp3	Matrix metallopeptidase 3	4.81
Slfn4	Schlafen 4	4.75
Sestd1	SEC14 and spectrin domains 1	4.71
Gm7609	Predicted gene 7609	4.69
Cpxm1	Carboxypeptidase X 1 (M14 family)	4.65
Padi4	Peptidyl arginine deiminase, type IV	4.64
Itgb6	Integrin β6	4.63
Srgn	Serglycin	4.59
Gm7609	Predicted gene 7609	4.58
Cd200r3	CD200 receptor 3	4.56
Clec4n	C-type lectin domain family 4, member n	4.52
H2-Q6	Histocompatibility 2, Q region locus 6	4.49
Csprs	Component of Sp100-rs	4.39
Nfkbie	Nuclear factor of κ light polypeptide gene enhancer in B-cells inhibitor, epsilon	4.38
Mgat3	Mannoside acetylglucosaminyltransferase 3	4.32
Clca1	Chloride channel calcium activated 1	4.29
Ces3	Carboxylesterase 3	4.29
Car8	Carbonic anhydrase 8	4.29
Tnf	Tumor necrosis factor	4.28
Csprs	Component of Sp100-rs	4.26
Wbscr17	Williams-Beuren syndrome chromosome region 17 homolog (human)	4.18
Gpnmb	Glycoprotein (transmembrane) nmb	4.17
Steap4	STEAP family member 4	4.13
Slc39a4	Solute carrier family 39 (zinc transporter), member 4	4.12
Cxcl2	Chemokine (C-X-C motif) ligand 2	4.10
Pglyrp1	Peptidoglycan recognition protein 1	4.04
Dram1	DNA-damage regulated autophagy modulator 1	3.97
Grid2	Glutamate receptor, ionotropic, delta 2	3.94
Atp6v0d2	ATPase, H^+ transporting, lysosomal V0 subunit D_2	3.90
Itga2	Integrin α2	3.85
Il1f9	Interleukin 1 family, member 9	3.85
Capsl	Calcyphosine-like	3.84
Pmepa1	Prostate transmembrane protein, androgen induced 1	3.80
Clec5a	C-type lectin domain family 5, member a	3.78
Dclk1	Doublecortin-like kinase 1	3.73
S100a9	S100 calcium binding protein A9 (calgranulin B)	3.71
Gp49a	Glycoprotein 49 A	3.69
Ly6k	Lymphocyte antigen 6 complex, locus K	3.65
Mpeg1	Macrophage expressed gene 1	3.64
Il1b	Interleukin 1β	3.62
Cxcr4	Chemokine (C-X-C motif) receptor 4	3.60
Eya2	Eyes absent 2 homolog (*Drosophila*)	3.59
Tyrobp	TYRO protein tyrosine kinase binding protein	3.59
Pdgfrl	Platelet-derived growth factor receptor-like	3.58
Sfrp1	Secreted frizzle-related protein 1	3.54
Casp1	Caspase 1	3.54
Gda	Guanine deaminase	3.54
Nfkbia	Nuclear factor of κ light polypeptide gene enhancer in B-cells inhibitor, α	3.52
Gsdmc2	Gasdermin C2	3.49
Nedd9	Neural precursor cell expressed, developmentally downregulated gene 9	3.49
Frzb	Frizzle-related protein	3.49
Arl14	ADP-ribosylation factor-like 14	3.49
Gm7609	Predicted gene 7609	3.47
Krt7	Keratin 7	3.47
Ubd	Ubiquitin D	3.45
Fcrls	Fc receptor-like S, scavenger receptor	3.45
Mmp12	Matrix metallopeptidase 12	3.45
Serpinb11	Serine (or cysteine) peptidase inhibitor, clade B (ovalbumin), member 11	3.44
Tgtp	T-cell–specific GTPase	3.43
Lyz2	Lysozyme 2	3.38

Table W4. The 100 Most Downregulated Genes in the Microarray Study Comparing PE–PTEN+/–IKK2ca/ca to PE–PTEN+/–.

Gene Symbol	Full Name	Fold Expression
Spink3	Serine peptidase inhibitor, Kazal type 3	0.00
Sbp	Spermine binding protein	0.01
Wfdc3	WAP four-disulfide core domain 3	0.02
Pnliprp1	Pancreatic lipase-related protein 1	0.02
Spink5	Serine peptidase inhibitor, Kazal type 5	0.03
4930408F14Rik	RIKEN cDNA 4930408F14 gene	0.04
4930408F14Rik	RIKEN cDNA 4930408F14 gene	0.04
4930408F14Rik	RIKEN cDNA 4930408F14 gene	0.04
Syt10	Synaptotagmin X	0.04
4930408F14Rik	RIKEN cDNA 4930408F14 gene	0.05
Abo	ABO blood group (transferase A, α 1-3-*N*-acetylgalactosaminyltransferase, transferase B, α 1-3-galactosyltransferase)	0.05
Eapa2	Experimental autoimmune prostatitis antigen 2	0.05
Pbsn	Probasin	0.06
G6pc2	Glucose-6-phosphatase, catalytic, 2	0.06
9530002B09Rik	RIKEN cDNA 9530002B09 gene	0.06
Derl3	Der1-like domain family, member 3	0.06
Azgp1	α-2-Glycoprotein 1, zinc	0.07
Atp12a	ATPase, H^+/K^+ transporting, nongastric, α polypeptide	0.07
4930408F14Rik	RIKEN cDNA 4930408F14 gene	0.07
Defb10	Defensin β10	0.07
Tgm4	Transglutaminase 4 (prostate)	0.07
4930408F14Rik	RIKEN cDNA 4930408F14 gene	0.07
D030018L15Rik	Nuclear receptor coactivator 2 pseudogene	0.07
4930408F14Rik	RIKEN cDNA 4930408F14 gene	0.08
Pcp4	Purkinje cell protein 4	0.08
4930408F14Rik	RIKEN cDNA 4930408F14 gene	0.08
Gm5615	Predicted gene 5615	0.08
Defb1	Defensin β1	0.09
Ceacam2	Carcinoembryonic antigen–related cell adhesion molecule 2	0.09
Hmgcs2	3-Hydroxy-3-methylglutaryl-coenzyme A synthase 2	0.09
Htr3a	5-Hydroxytryptamine (serotonin) receptor 3A	0.09
Atp6v1c2	ATPase, H^+ transporting, lysosomal V1 subunit C2	0.09
Cyp3a57	Cytochrome P450, family 3, subfamily a, polypeptide 57	0.10
Agtr1a	Angiotensin II receptor, type 1a	0.10
Mme	Membrane metalloendopeptidase	0.10
Prom2	Prominin 2	0.10
Aass	Aminoadipate-semialdehyde synthase	0.11
Slc9a2	Solute carrier family 9 (sodium/hydrogen exchanger), member 2	0.11
Epha3	Eph receptor A3	0.11
Smgc	Submandibular gland protein C	0.11
Decaf12l1	DDB1 and CUL4 associated factor 12-like 1	0.11
Myh11	Myosin, heavy polypeptide 11, smooth muscle	0.12
Acrbp	Proacrosin binding protein	0.12
Apof	Apolipoprotein F	0.12
Nkx2-6	NK2 transcription factor related, locus 6 (*Drosophila*)	0.12
Hhip	Hedgehog-interacting protein	0.12
Egf	Epidermal growth factor	0.12
Uph1	Ureidopropionase, β	0.13
Prlr	Prolactin receptor	0.13
Spc25	SPC25, NDC80 kinetochore complex component, homolog (*S. cerevisiae*)	0.13
Nkx3-1	NK-3 transcription factor, locus 1 (*Drosophila*)	0.13
Hpgd	Hydroxyprostaglandin dehydrogenase 15 (NAD)	0.13
Prlr	Prolactin receptor	0.14
Gpr165	G protein–coupled receptor 165	0.14
Cbs	Cystathionine β-synthase	0.14
Slc30a10	Solute carrier family 30, member 10	0.14
Bmpr1b	Bone morphogenetic protein receptor, type 1B	0.14
Fcgbp	Fc fragment of IgG binding protein	0.15
Fam38b2	Family with sequence similarity 38, member B2	0.15
Srd5a2	Steroid 5 α-reductase 2	0.15
Fam38b	Family with sequence similarity 38, member B	0.15
Cdh8	Cadherin 8	0.15
Spink11	Serine peptidase inhibitor, Kazal type 11	0.16
Gabra4	γ-Aminobutyric acid (GABA) A receptor, subunit α 4	0.16
Abca5	ATP-binding cassette, subfamily A (ABC1), member 5	0.16
Pdzk1	PDZ domain containing 1	0.16
Slc30a2	Solute carrier family 30 (zinc transporter), member 2	0.16
Acvr1c	Activin A receptor, type IC	0.17
H2-Q10	Histocompatibility 2, Q region locus 10	0.17
Fah	Fumarylacetoacetate hydrolase	0.17
Bhlha15	Basic helix-loop-helix family, member a15	0.17
Slc26a4	Solute carrier family 26, member 4	0.17
Cckar	Cholecystokinin A receptor	0.17
Cnn1	Calponin 1	0.18
Wif1	Wnt inhibitory factor 1	0.18
Ggt1	γ-Glutamyltransferase 1	0.18
Cyp2j13	Cytochrome P450, family 2, subfamily j, polypeptide 13	0.18
Slc5a3	Solute carrier family 5 (inositol transporters), member 3	0.18
Otud7a	OTU domain containing 7A	0.18
Gm1574	Predicted gene 1574	0.19
Defb50	Defensin β50	0.19
Slc18a1	Solute carrier family 18 (vesicular monoamine), member 1	0.20
Chn2	Chimerin (chimaerin) 2	0.20
Tmem45a	Transmembrane protein 45a	0.20
Man1a	Mannosidase 1, α	0.20
Spink8	Serine peptidase inhibitor, Kazal type 8	0.20
Glb1l3	Galactosidase, β1 like 3	0.20
5430419D17Rik	RIKEN cDNA 5430419D17 gene	0.21
9130230L23Rik	RIKEN cDNA 9130230L23 gene	0.21
Fam115c	Family with sequence similarity 115, member C	0.21
Myl9	Myosin, light polypeptide 9, regulatory	0.21
Rab39b	RAB39B, member RAS oncogene family	0.21
Ms4a5	Membrane-spanning 4 domains, subfamily A, member 5	0.22
Gnmt	Glycine *N*-methyltransferase	0.22
P2rx1	Purinergic receptor P2X, ligand-gated ion channel, 1	0.22
Doc2b	Double C2, β	0.22
BC005685	cDNA sequence BC005685	0.22
Bmp7	Bone morphogenetic protein 7	0.22
BC005685	cDNA sequence BC005685	0.22
Upk1a	Uroplakin 1A	0.22
Nxf7	Nuclear RNA export factor 7	0.22
Rnase1	Ribonuclease, RNase A family, 1 (pancreatic)	0.23
BC005685	cDNA sequence BC005685	0.23
Ndrg2	N-*myc* downstream regulated gene 2	0.23
Slco4c1	Solute carrier organic anion transporter family, member 4C1	0.23
Gpr110	G protein–coupled receptor 110	0.23
Slc22a1	Solute carrier family 22 (organic cation transporter), member 1	0.23
Proc	Protein C	0.24
Acrv1	Acrosomal vesicle protein 1	0.24
Aldh6a1	Aldehyde dehydrogenase family 6, subfamily A1	0.25

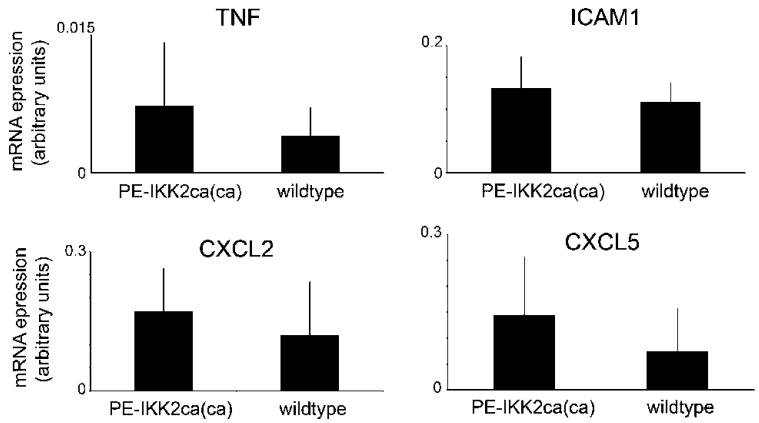

Figure W4. Quantitative PCR analysis of NF-κB–dependent target genes in IKK2ca(ca) lateral prostates compared with wild-type (12 months; $n = 5$ per group). Error bars, SEM.

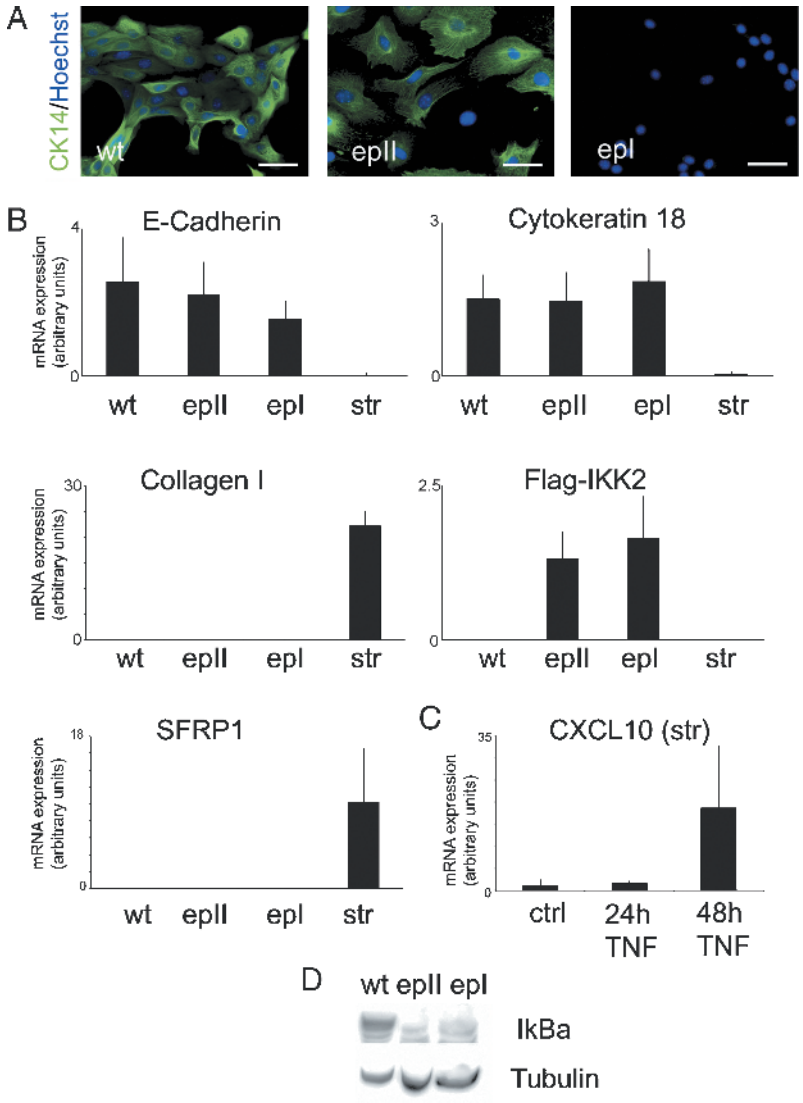

Figure W5. Expression of epithelial and stromal markers in epithelial and stromal cell lines. (A) Colored image of cytokeratin 14 (CK14) staining of indicated epithelial cell lines in culture. Green indicates CK14 signal; blue, Hoechst signal. Scale bars, 50 μm. (B) Expression profile of epithelial and stromal cell lines. The mRNA expression was determined by quantitative RT-PCR. (C) Expression of CXCL10 mRNA in the stromal cell line (str) on treatment with TNF (10 ng/ml). Ctrl indicates control cells (untreated). (D) Western blot showing degradation of IκBα in transgenic cells, indicating IKK2 activity.